Electronic Supplementary Information

Reducing Noble Metal Dependence: Oxygen Evolution Reaction with Ru-Minimized $Bi_2Ru_2O_7$@MOF-801 Composite

P Sujita†[a] , Keshav Gupta†[b], , V Gopal[a], S Sarmila[a], Sethumathavan Vadivel*[a]

Supplementary equations

Equation S1. $iR\ correction = E_{Hg/HgO} - E_{iR}$

Hg/HgO - Mercury Mercuric oxide

iR - current x resistance

E - potential

Equation S2. $E_{RHE} = \left(E_{Hg/HgO} - E_{iR}\right) + 0.924\ V$

RHE - Reversible hydrogen electrode

Equation S3. $\eta_a(OER) = E_{RHE} - 1.23\ V$

η - overpotential

OER - Oxygen evolution reaction

a - current density (50 mA cm^{-2} and 100 mA cm^{-2})

Equation S4. $\frac{1}{C^2} = -\omega Z_i^{\,2} \forall\ \omega = 2\pi\vartheta$

C - Capacitance

ω - angular frequency

υ - linear frequency

Equation S5. $2C_{dl} = \frac{\Delta j}{\vartheta}$

C_{dl} - double layer capacitance

Δj - difference in current density

υ - scan rate

Equation S6. $ECSA = \frac{C_{dl}}{C_s}$

ESCA - electrochemical active surface area

C_s - specific capacitance

Supplementary notes

Note S1. Materials used and origin

Bismuth nitrate, ruthenium chloride, sodium hydroxide, activated carbon, and PVDF were purchased from Merck. Acetone, ethylene glycol, formic acid, potassium hydroxide from Qualigens. DABCO, zirconium chloride, and fumaric acid were procured from TCI. NMP, ethanol, and dimethyl formamide from SRL chemicals. Nickel foam was procured from Wee Scientific, India.

Note S2. Material characterization

The crystal structure of the samples was examined using a PANalytical X-ray diffractometer (Cu Kα radiation) from the Netherlands. Functional groups within the material were identified through Fourier Transform Infrared (FTIR) spectroscopy, performed with a SHIMADZU IRTracer-100. The materials' morphology was investigated via field-emission scanning electron microscopy (FESEM) on a Carl Zeiss EVO18, which also featured energy-dispersive X-ray spectroscopy (EDS), and high-resolution transmission electron microscopy (HRTEM) from JEOL, Japan. Additionally, X-ray photoelectron spectroscopy (XPS) from Physical Electronics was utilized to analyze the surface chemical composition and electronic states of the samples.

Note S3. Preparation of working electrode

Ni-foam of dimension 3 cm * 3 cm (length * breadth) was pretreated with dilute HCl and washed with water and distilled water. The treated Ni-foam was dried at 60 °C for 2 h. A slurry was made with active material, binder (PVDF), and conducting material (AC) of weight ratio 8:1:1 with the help of NMP solvent. The slurry was coated on the 1 cm * 1 cm part of the Ni-foam and dried in a hot air oven.

Note S4. Electrochemical characterization

An OrigaLys electrochemical potentiostat (model OGF05A, France) with a three-electrode setup was used for the electrochemical investigations. A Hg/HgO electrode was utilized as the reference electrode, Pt wire as the counter electrode, and the modified Ni foam as the working electrode with 1 M KOH as electrolyte. The reference electrode was calibrated to 0.924V with Pt wire as both the working electrode and counter electrode and 1M KOH as the electrolyte. The calibrated reference electrode potential was used for reversible hydrogen electrode (RHE) conversion. Further, the as-prepared electrocatalyst

was examined for OER activity with the help of electro-analytical tools such as linear sweep voltammetry (LSV), cyclic voltammetry (CV), electrochemical impedance spectroscopy (EIS), Chronoamperometry (CA) and EIS Mott Schottky (EIS-MS). LSV and CV were extensively used for accessing the activity of the catalyst, working electrode activation, and accessing electrical double-layer formation at various scan rates. The results were presented with iR drop correction against the RHE. EIS was conducted with a frequency sweep of 100 kHz to 10 mHz with DC potential beyond the onset against the Hg/HgO scale. CV analysis was employed in non-faradaic regions in different scan rates from 10 mV s^{-1} to 250 mV s^{-1}. The stability of the material accessed through CA with 1.2 V vs. Hg/HgO for 24 h. Mott Schottky analysis was performed with a frequency of 200 Hz.

Supplementary calculation

Calculation S1. Weight percentage calculation of Ru in $Bi_2Ru_2O_7$@MOF-801 composite

The total mass of the composite 50 mg $Bi_2Ru_2O_7$ + 20 mg MOF-801 = 70 mg

Percentage of $Bi_2Ru_2O_7$ in composite = (50 / 70) × 100 = 71.43 %

Percentage of MOF-801 in composite = (20 / 70) × 100 = 28.57 %

Molar mass of $Bi_2Ru_2O_7$ is 732.1 g/mol.

The mass contribution of ruthenium in $Bi_2Ru_2O_7$ is:

Mass of Ru = 2×101.07=202.14 g/mol

The weight percentage of Ru in $Bi_2Ru_2O_7$ = (202.14 / 732.1) × 100 = 27.6%.

As calculated earlier, **27.6%** of the mass of $Bi_2Ru_2O_7$ is ruthenium.

Mass of Ru in $Bi_2Ru_2O_7$ = 50 mg × (27.6 /100) = 13.8mg

Weight Percentage of Ru in the composite = (13.8 / 70) × 100 = 19.7%

Calculation S2. ECSA calculation from C_{dl}

$$ECSA = \frac{C_{dl}}{C_s}$$

C_s is 40 µF

$Bi_2Ru_2O_7$ = $\frac{10.56\ mF}{40\ \mu F} = \frac{10.56\ mF}{40\ mF} \times 1000 = 264\ cm^2$

MOF-801 = $\frac{4.94\ mF}{40\ \mu F} = \frac{4.94\ mF}{40\ mF} \times 1000 = 123.5\ cm^2$

$Bi_2Ru_2O_7$ @MOF-801 = $\frac{13.3\ mF}{40\ \mu F} = \frac{13.3\ mF}{40\ mF} \times 1000 = 332.5\ cm^2$

Supplementary images

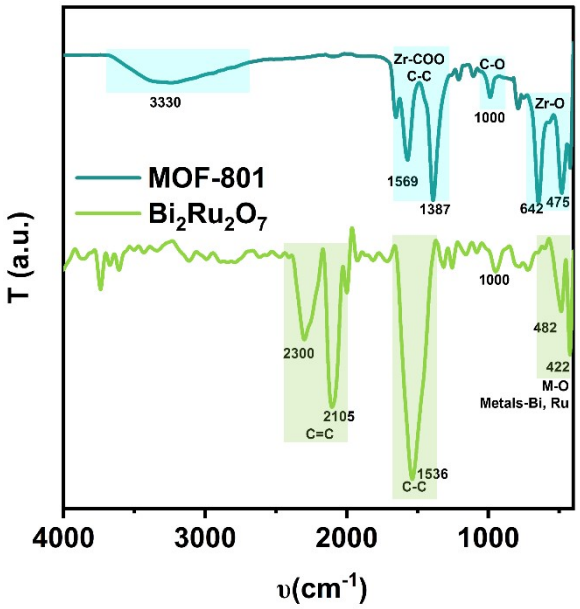

Figure S1. FTIR spectra of $Bi_2Ru_2O_7$, and MOF-801.

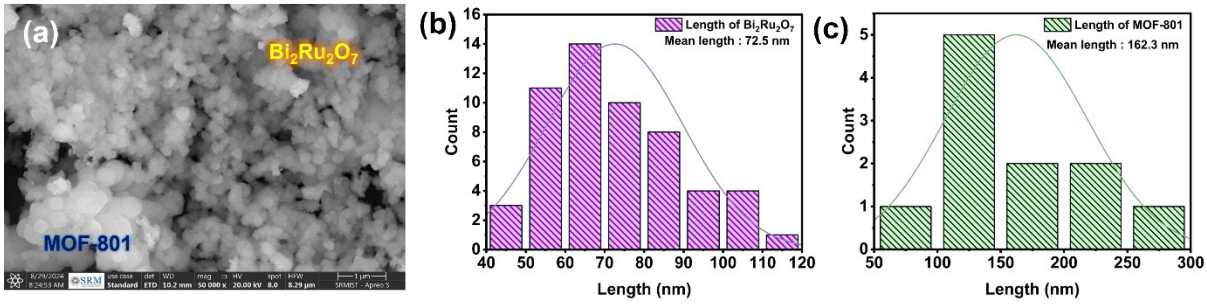

Figure S2. (a) SEM image of $Bi_2Ru_2O_7$@MOF-801 composite, (b) Size distribution histogram of $Bi_2Ru_2O_7$ and (c) MOF-801

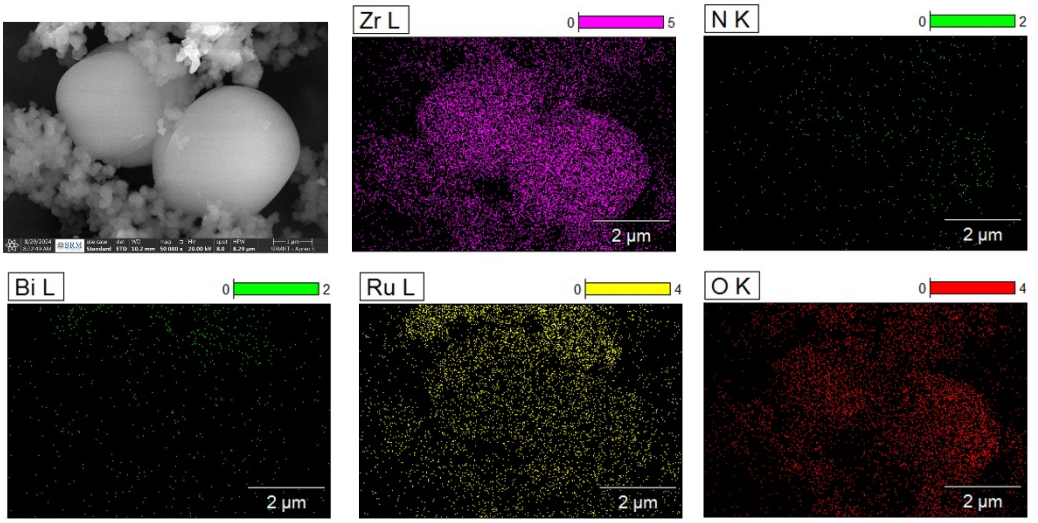

Chemical Formula	Weight %	Atom %
C	8.68	19.33
N	1.75	3.33
O	38.46	64.27
Zr	30.10	8.82
Ru	11.42	3.02
Bi	9.60	1.23
	100.00	100.00

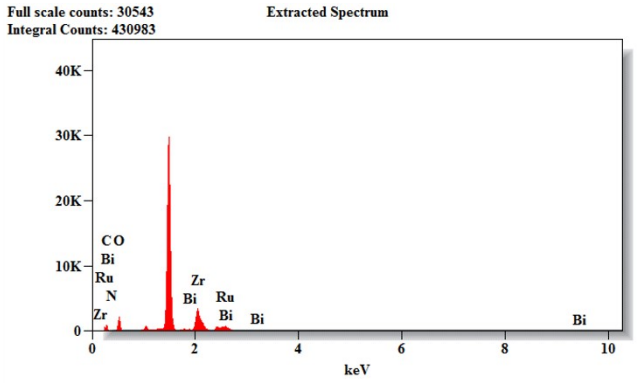

Figure S3. Elemental distribution spectroscopy images of $Bi_2Ru_2O_7$@MOF-801 composite from SEM analysis.

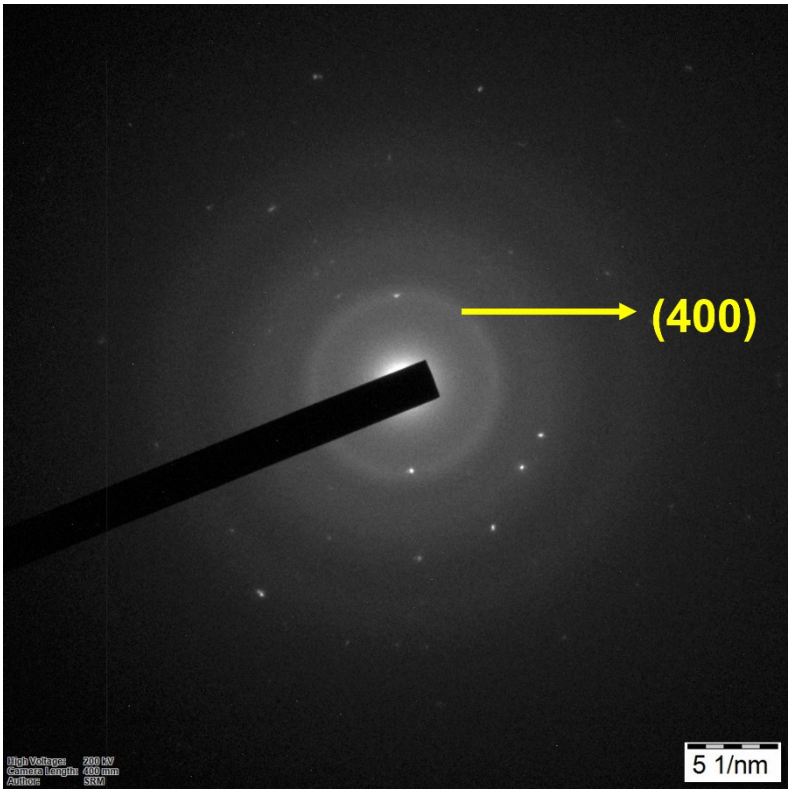

Figure S4. Selected area electron diffraction (SAED) pattern of $Bi_2Ru_2O_7$@MOF 801 composite from TEM analysis.

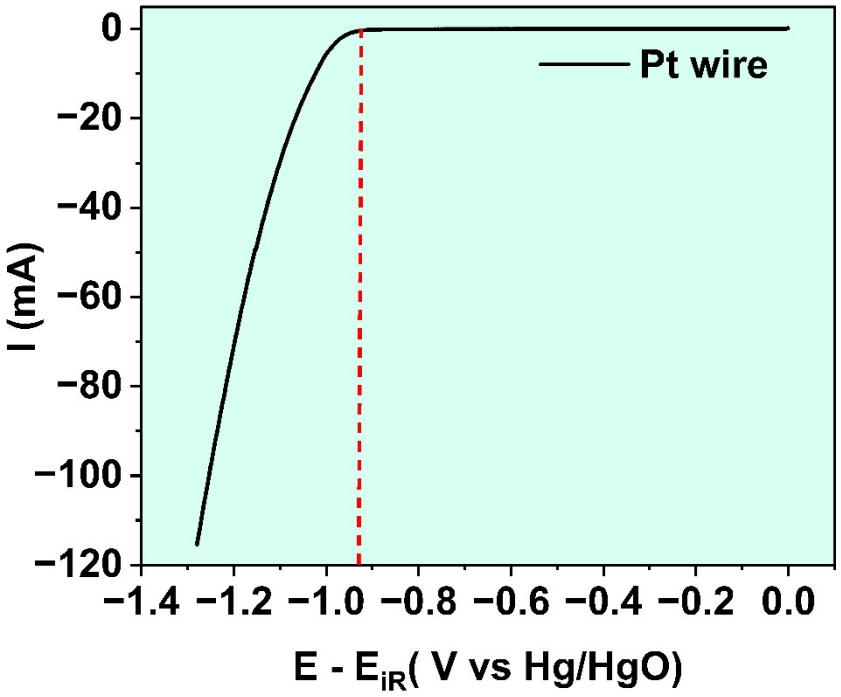

Figure S5. Calibration curve of Pt-wire

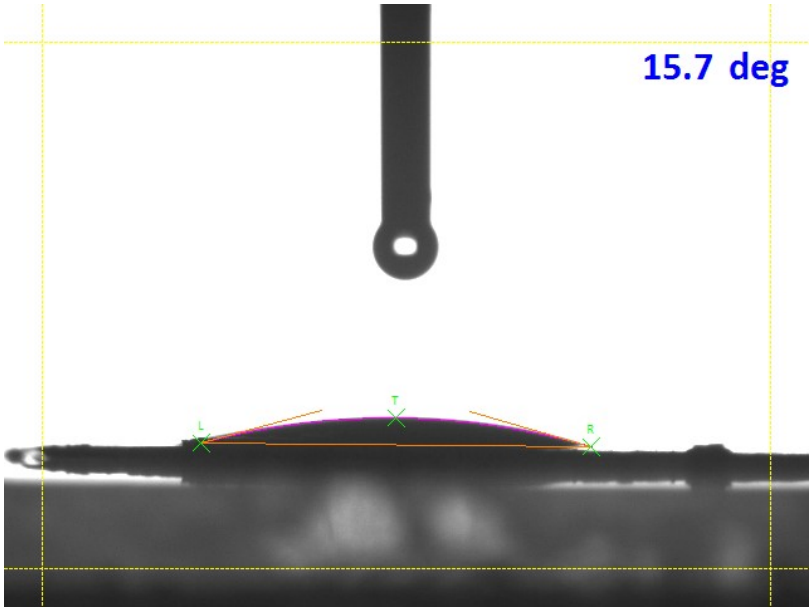

Figure S6. Surface water contact angle of MOF-801

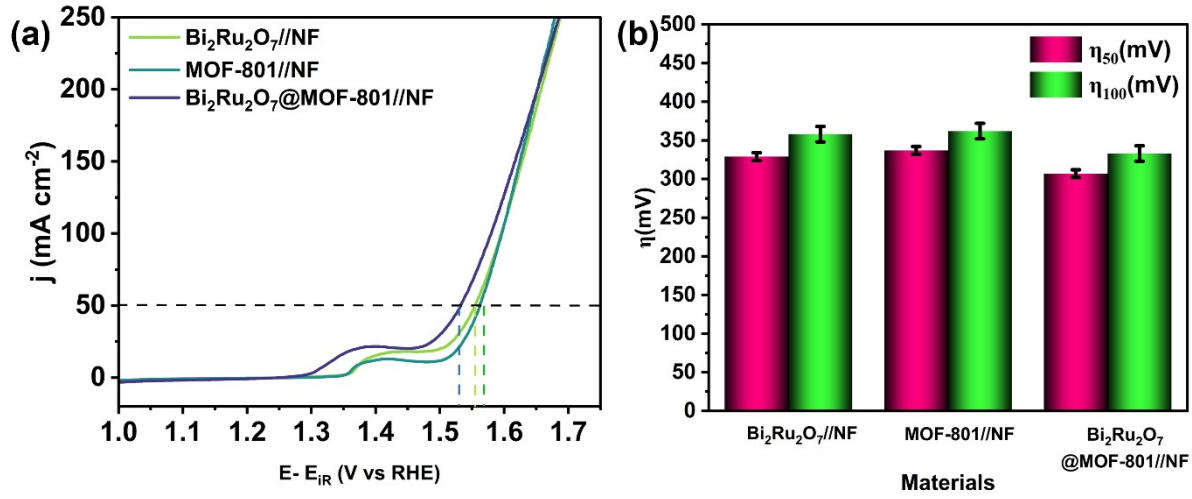

Figure S7. (a) Polarization curves of $Bi_2Ru_2O_7$//NF, MOF-801//NF, $Bi_2Ru_2O_7$@MOF-801//NF (reproducibility) and (b) Overpotentials observed at 50 mA cm^{-2} (η_{50}), and 100 mA cm^{-2} (η_{100}) with reproducible error bar.

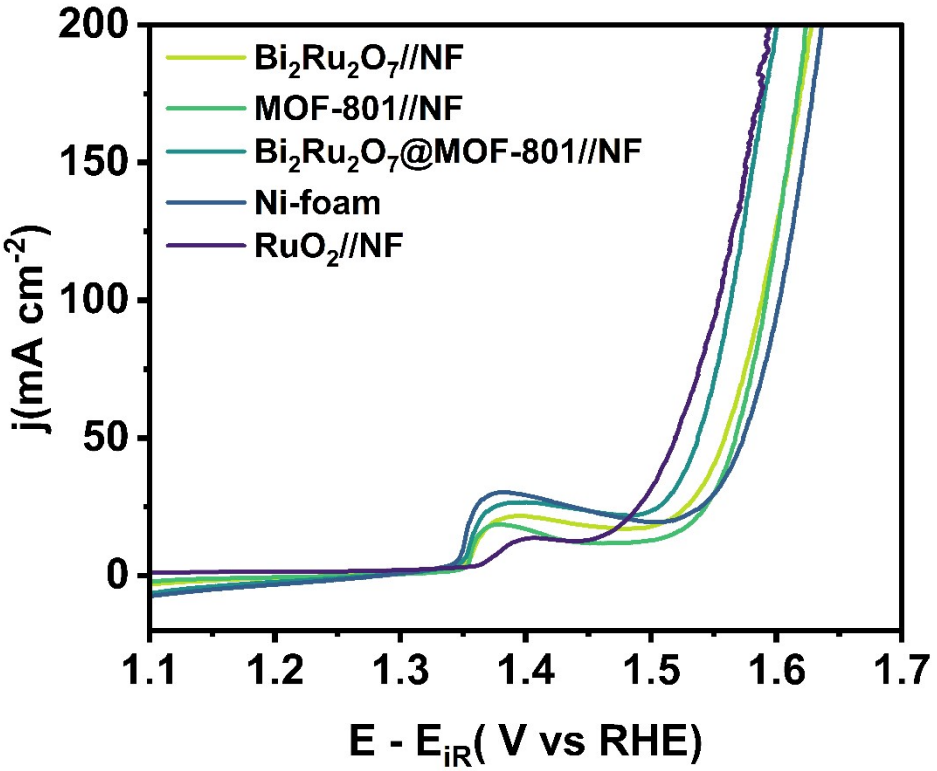

Figure S8. The polarization curves for $Bi_2Ru_2O_7$//NF , MOF-801//NF , $Bi_2Ru_2O_7$@MOF-801//NF , Ni-foam and RuO_2//NF

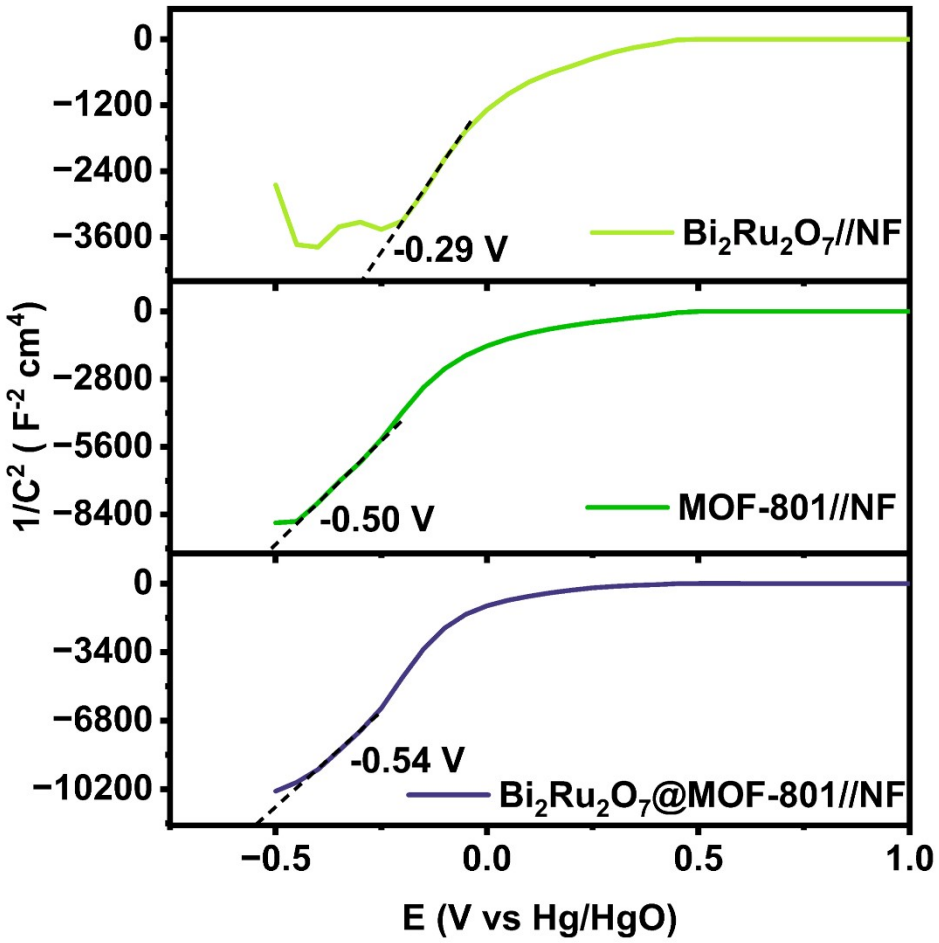

Figure S9. Mott-Schottky plot for $Bi_2Ru_2O_7$//NF , MOF-801//NF , and $Bi_2Ru_2O_7$@MOF-801//NF at 200 Hz

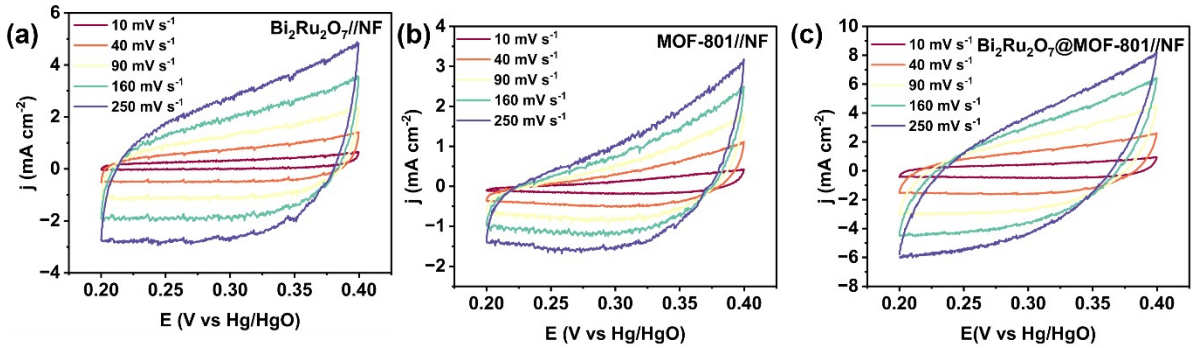

Figure S10. CV profiles of $Bi_2Ru_2O_7$//NF, MOF-801//NF, and $Bi_2Ru_2O_7$@MOF-801//NF in various scan rates (10mV s^{-1}, 40mV s^{-1},90mV s^{-1},160mV s^{-1}, and 250mV s^{-1}).

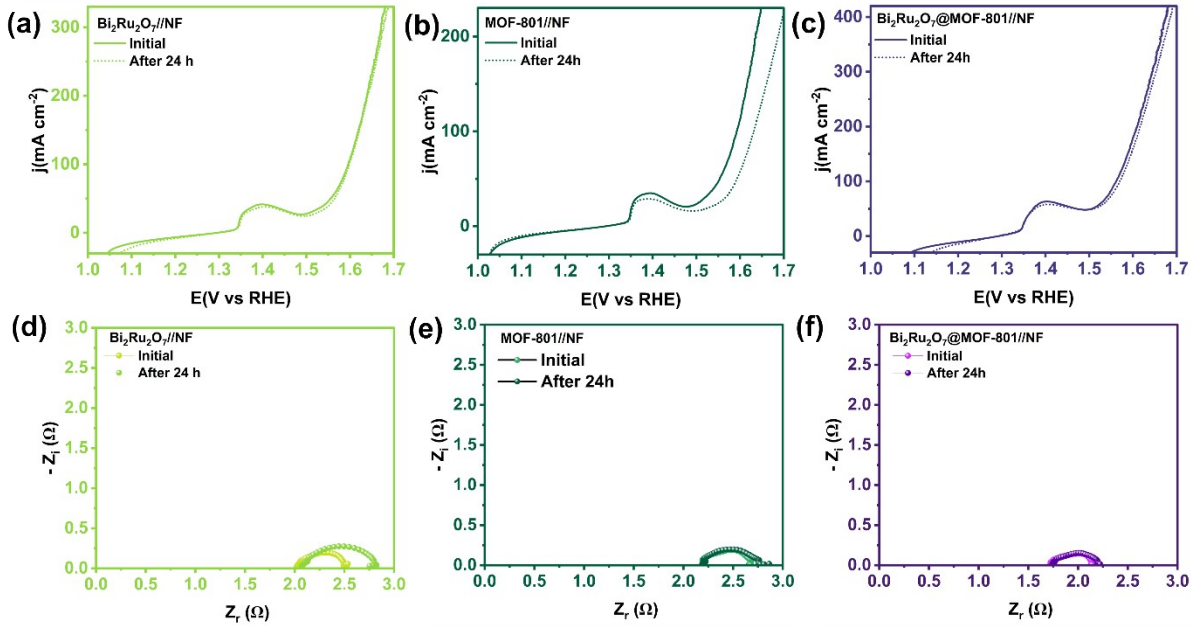

Figure S11. The LSV curves and Nyquist plots for pre- and post-stability 24 h chronoamperometry analysis of $Bi_2Ru_2O_7$//NF, MOF-801//NF, and $Bi_2Ru_2O_7$@MOF-801//NF